Structure and Properties of Tailor-Made Poly(ethyl acrylate)/Clay Nanocomposites Prepared by *In Situ* Atom Transfer Radical Polymerization

Haimanti Datta, Nikhil K. Singha, Anil K. Bhowmick

Rubber Technology Centre, Indian Institute of Technology, Kharagpur 721302, India

Received 2 May 2007; accepted 7 August 2007
DOI 10.1002/app.27760
Published online 19 February 2008 in Wiley InterScience (www.interscience.wiley.com).

ABSTRACT: An in-depth study was carried out on the structure and properties of a series of poly(ethyl acrylate)/clay nanocomposites prepared by *in situ* atom transfer radical polymerization (PNCIs) with well-defined molecular weights and narrow molecular weight distributions. Wide-angle X-ray diffraction and transmission electron microscopy studies revealed an exfoliated clay morphology, whereas conventional solution blending generated an intercalated structure. The storage moduli of the PNCIs showed a moderate increase over that of the neat polymer [poly(ethyl acrylate)]. The sample containing 4 wt % clay (PNCI4, where the number following PNCI indicates the weight percentage of clay) exhibited the highest improvement (31.9% at 25°C). In PNCIs, the β-transition temperature showed a remarkable decrease (by 175% in PNCI4) along with a shift toward higher temperatures. This indicated the probability of the anchoring of the −OH group of the clay layers to the >C=O group of the pendant acrylate moiety, which was also confirmed by Fourier transform infrared analysis. Rheological measurements indicated a significant increase in the shear viscosity [by 9% in PNCI2, 15% in PNCI4, and 6% in the poly(ethyl acrylate)/clay nanocomposite with 2 wt % clay prepared by solution blending]. The PNCIs registered enhanced thermal stability, as indicated by the shift in the peak maximum temperature (388 and 392°C for the neat polymer and PNCI4, respectively) and a decrease in the rate of degradation (by 3.5% in PNCI2, 10.2% in PNCI4, and 49.3% in PNCI6). © 2008 Wiley Periodicals, Inc. J Appl Polym Sci 108: 2398–2407, 2008

Key words: atom transfer radical polymerization (ATRP); living polymerization; mechanical properties; nanocomposites; organoclay

INTRODUCTION

In recent years, great attention has been paid to polymer–clay nanocomposites by both the academic and industrial communities because of the significant improvement in the physical properties of the host polymer matrix.[1–5] The salient feature that leads to such improvements is the significant disruption of individual silicate layers in a polymer matrix with nanoscopic dimensions (exfoliated structure). However, in most cases, silicate layers are not randomly distributed; instead, an interlayer expansion occurs, and polymer chains penetrate inside this interlayer region, which, hence, maintains the hierarchical architecture of clay tactoids (intercalated structure). The synthesis of exfoliated nanocomposites is of particular interest, as these usually provide the best enhancement in properties and involve maximum matrix–filler interactions because of the large aspect ratio and surface area of the clay.

Organoclay nanocomposites are prepared primarily by three methods: (1) solution blending, (2) melt intercalation, and (3) *in situ* polymerization. Solution blending involves the mixing of clay with a solution of polymer. The structure of the resulting nanocomposite depends on the molecular interactions between the polymer and the clay surface, the solution concentration, the nature of solvent, and the subsequent energy reduction.[6–11] In melt intercalation, a mixture of polymer and clay, heated above the glass-transition temperature (T_g) or melting temperature of the polymer, is mixed with shear forces in an extruder.[12,13] However, compared to the previous two processes, the literature on intercalating monomers into clay followed by polymerization (i.e., *in situ* polymerization) is scanty. This method has an advantage over the other two in that it can provide a high degree of exfoliation of the layered silicate aggregates in the nanocomposites. This is because the viscosity of the monomers is so low that they can easily intercalate the layered silicates.[1]

In the area of *in situ* polymerization methods, there have been very few investigations that have studied the production of polymers with well-defined molecular weights and narrow polydispersity indices.[14–18] A diversity of low-molecular-weight acrylic polymers and copolymers find potential use in the development of high-performance coating applications.[19–21] Moreover, the molecular weight

Correspondence to: A. K. Bhowmick (anilkb@rtc.iitkgp.ernet.in).

distribution (MWD) of a polymer is one of its most fundamental characteristics. Properties such as flow behavior (rheology), reactivity, degree of curing, hardness, strength, and many physical properties (weathering behavior, crack resistance, permeability for gases and liquids, etc.) are influenced by the MWD of the polymer.[22] A narrow MWD also causes a smoother hardening during the curing phase, which allows the optimization of the resulting film properties.[18] Atom transfer radical polymerization (ATRP) is a living free-radical polymerization technique, developed in recent years,[23–27] that leads to the preparation of tailor-made polymers with predictable molecular weights and narrow MWDs. The success of this polymerization method arises from its synthetic simplicity, versatility, compatibility with a broad range of functional groups, and tolerance toward water and other protic solvents.

An added advantage includes the living nature of the polymerization, because of which further sequential addition of monomers is possible to optimally fine-tune the properties of the resulting polymer to end applications. The functionalized chain end can also be used to synthesize a macroinitiator. The development of low-molecular-weight polymer–clay nanocomposites based on this approach is particularly appealing because low-molecular-weight polymers are more advantageous in the wetting of reinforcing elements than polymers of high molecular weight.[28] However, there has been no report on *in situ* poly(ethyl acrylate)–clay nanocomposites (PNCs), except for one published by our group based on a conventional radical polymerization approach.[6]

In this study, we prepared poly(ethyl acrylate) (PEA)/organic clay nanocomposites by *in situ* ATRP with well-defined molecular weights and narrow polydispersity indices. The structure of the resulting nanocomposites was examined with wide-angle x-ray diffraction (WAXD), scanning electron microscopy, and transmission electron microscopy (TEM). Also, a comparison was made with composites created by conventional solution blending. The molecular weights of PEA extracted from PNC materials were determined by gel permeation chromatography (GPC) analyses with tetrahydrofuran as the eluant. We also studied the effect of organoclay loading on the mechanical, rheological, and thermal properties of the nanocomposites.

EXPERIMENTAL

Materials

Ethyl acrylate (Aldrich, Milwaukee, WI, 99%) was washed twice with an aqueous solution of sodium hydroxide (5%) and twice with distilled water. The organic portion was dried with sodium carbonate (anhydrous) by overnight stirring, then filtered, and finally distilled under reduced pressure over calcium hydride. The distillates were stored at −18°C before they were used. CuBr (Aldrich, Milwaukee, WI, 98%) was stirred with glacial acetic acid for 12 h, washed with ethanol and diethyl ether, and then dried *in vacuo* at 75°C for 3 days. The purified CuBr was stored in a nitrogen atmosphere. Methyl 2-bromopropionate (Alfa Aesar, Karlsruhe, Germany, 97%), 2,2′-bipyridine (Lancaster, Morecambem, England, 98%), and all other chemicals were used as received. Nanoclay, Cloisite 30B, with a surfactant (methyl tallow-bis-2-hydroxy ethyl quaternary ammonium), was supplied by Southern Clay Products (Gonzales, TX). The chemical structure of the surfactant is given below:

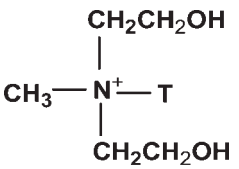

MT2EtOH

In the previous structure, N^+ denotes quaternary ammonium chloride, and T denotes tallow consisting of about 65% C18, about 30% C16, and about 5% C14. According to the Technical Properties Bulletin from Southern Clay Products, the amount of surfactant (methyl tallow-bis-2-hydroxy ethyl quaternary ammonium) residing at the surface of Cloisite 30B was 90 mequiv/100 g.

Polymerization procedure

In situ ATRP

The required amount of nanoclay was placed in a test tube (8 × 2.5 cm^2) provided with a B-14 standard joint and dispersed in the monomer, ethyl acrylate (5 g, 4.9×10^{-2} mol; already degassed by purging with nitrogen for 30 min before use), under a nitrogen atmosphere for 10 h. CuBr (0.0716 g, 4.9×10^{-4} mol) was added. It was then purged with nitrogen for 15 min. The ligand, bipyridine (0.1558 g, 9.8×10^{-4} mol), and finally, the initiator, methyl 2-bromopropionate (0.0834 g, 4.9×10^{-4} mol), were added to the test tube in sequential order via a dry and purified syringe at ambient temperature with continuous stirring. The reaction vessel was sealed with a rubber septum, which was secured by Cu wire and was immersed into an oil bath maintained at a temperature of 90°C and stirred. After a specific time (5.5 h), the reaction was quenched by cooling of the solution. We removed residual copper catalyst by passing the solution through a column of neutral alumina oxide. The final polymer was dried in a

vacuum oven at 45°C. The targeted degree of polymerization (DP) was kept at 100 [DP = $\Delta[M]/[I]_o$, i.e., the amount of monomer consumed ($\Delta[M]$) per initiator molecule added to the reaction ($[I]_o$)] in all cases. The choice of optimized reaction conditions and ingredients were taken from an earlier study,[29] where we carried out the homopolymerization and block copolymerization of ethyl acrylate with well-defined molecular weights and narrow MWDs.

Solution blending

The virgin polymer, PEA, prepared by ATRP (molecular weight 7230), was first dissolved in a solvent, ethyl alcohol. The nanoclay was also dispersed in the same solvent (by 2 wt % with respect to PEA) at room temperature for 2 h. The clay dispersion was subsequently added to the polymer solution, and the mixture was agitated for an additional 2 h to make a homogeneous mixture. The solution was then dried in a vacuum oven at 50°C for 2 days to drive out the solvents.

Table I reports the different modes of sample preparation with various clay loadings and their designations.

TABLE I
Sample Designation with Respect to the Mode of Preparation and Clay Loading

Sample	Mode of sample preparation	Clay loading (wt %)
PEA	ATRP	0
PNCSL2	Solution blending	2
PNCI2	*In situ* ATRP	2
PNCI4	*In situ* ATRP	4
PNCI6	*In situ* ATRP	6

Characterization

GPC

The molecular weights and MWDs of the polymers were determined by GPC at ambient temperature with a Waters model 510 high performance liquid chromatography pump, a Waters series R-400 differential refractometer, and Waters Ultrastyragel columns with pore sizes of 10,000, 1000, and 500 Å, which were preceded by a prefilter. Tetrahydrofuran was used as the eluant at a flow rate of 1.0 mL/min, and calibration was carried out with poly(methyl methacrylate) standards having low polydispersity indices. Before injection into the GPC system, the polymer solution was treated with the cation exchange resin Dowex 50 W (Fluka) to make it free from Cu salts. For the nanocomposite samples, the polymer was separated from the clay by high-speed ultracentrifugation and filtration through a 0.2-μm filter.

WAXD

X-ray diffraction analysis was performed with a Rigaku Dmax 2500 diffractometer with a Co target (λ = 0.179 nm) at room temperature. The system consisted of a rotating anode generator, operated at 40 kV and 30 mA of current, and a wide-angle goniometer. The samples were scanned from 2θ = 2–10° at the step scan mode (step size = 0.03°, preset time = 2 s), and the diffraction pattern was recorded with a scintillation counter detector.

Scanning electron microscopy and energy dispersive X-ray (EDX) silicon mapping

The dispersion of clay particles in the polymer matrices was studied with a Jeol JSM-5800 scanning electron microscope (Japan) operating at an accelerating voltage of 25 kV. The samples were sputter-coated with gold to avoid the artifacts associated with sample charging. The X-ray silicon mapping (EDX) of the hybrid composite materials was recorded on an Oxford EDAX system attached to the microscope.

TEM

The distribution of clay particles in the polymer matrix was studied with an high resolution transmission electron microscope (Jeol 2000, Japan) operated at an accelerated voltage of 200 kV. The samples were sectioned into sections about 100 nm thin −50°C with an ultracryomicrotome (Ultracut R, Leica) equipped with a glass knife. These cryotomed sections were then transferred to the copper grid and were observed through the microscope.

Dynamic mechanical thermal analysis

The dynamic mechanical properties of the polymers were measured with a dynamic mechanical analyzer (Viscoanalyzer VA 4000 150N, Metravib, Cedex, France). The samples were tested with an annular shear specimen holder, which allowed us to test the pasty sample and to follow it in a single test evolution from solid to pasty stage. The samples were heated from −50 to 50°C at a heating rate of 2°C/min at a constant frequency of 1 Hz. The storage modulus (G'), loss modulus (G''), and loss tangent ($\tan\delta$) were measured as a function of temperature for all of the samples under identical conditions.

Rheology

A stress controlled TA advanced rheometer (AR 2000) (Rheometrics, New Castle, DE) was used to measure the shear viscosity of the polymers in the cone and plate configuration with a Peltier plate

arrangement. The diameter of the plate was 40 mm, the truncation was 56 μm, and the cone angle was 1°59′50″. The data were collected with TA Rheology Advantage Data Analysis Software.

The flow behavior index (n) and consistency index (k) were calculated with the power-law model:[30]

$$\tau_{app} = k\dot{\gamma}^{n}_{app} \quad (1)$$

By definition

$$\eta_{app} = \tau_{app}/\dot{\gamma}_{app} \quad (2)$$

Therefore

$$\eta_{app} = k\dot{\gamma}^{n-1}_{app} \quad (3)$$

The logarithmic form for eq. (3) may be written as

$$\log \eta_{app} = \log k + (n-1)\log \dot{\gamma}_{app} \quad (4)$$

where τ_{app} is the apparent shear stress, $\dot{\gamma}_{app}$ is the apparent shear rate, and η_{app} is the apparent shear viscosity of the polymer materials.

The activation energy of flow was calculated on the basis of the Arrhenius equation:

$$\log \eta = \log A + E/RT \quad (5)$$

where A is a constant and η the coefficient of viscosity.

The E/R value was found for the slope of the plot of log viscosity versus $1/T$, from which the activation energy (E) was calculated. Here, T is the absolute temperature, and R is the Avogadro gas constant (8.315 J/mol).

Thermogravimetric analysis (TGA)

TGA of the neat polymer and the hybrid composites were recorded with a DuPont TGA instrument (model 2000) (Wilmington, DE). The measurements were performed from ambient temperature to 600°C at a programmed heating rate of 20°C/min under a nitrogen atmosphere. A sample weight of about 10 mg was used for all of the measurements.

RESULTS AND DISCUSSION

Molecular weights of virgin PEA and its nanocomposites

The molecular weights and MWDs of virgin PEA and various polymer samples extracted from its nanocomposites prepared by *in situ* ATRP [poly (ethyl acrylate)/clay nanocomposites prepared by *in situ* atom transfer radical polymerization (PNCIs)] were obtained by GPC analysis. The molecular weights of all of the samples displayed monomodal peak distributions corresponding to a molecular weight value predetermined by a suitable choice of the molar ratio of monomer to initiator. These values are shown in Table II. A good correlation between the theoretical (as calculated from the conversion of monomer) and experimental molecular weights was observed, which supported the controlled nature of the polymerization.

The molecular weights of the extracted polymers from the nanocomposites were only a little higher than that of the pristine polymer, which implied that the polymerization was not hindered at all in the presence of the foreign material, organoclay. The high values of initiator efficiency (I_{eff}) in all cases also supported this. This result was in contrast to the previously reported poly(vinyl alcohol)/clay nanocomposite prepared by conventional *in situ* free-radical polymerization,[31] where the polymerization was hindered in the intragallery region of organoclay, and number-average molecular weight (M_n) values decreased drastically with increasing clay content. The present study elucidated better control over molecular weight with the maintenance of the significantly narrower MWDs than the previously mentioned system.

WAXD studies

The X-ray diffractograms of the nanocomposites are shown in Figure 1(a–f) for neat PEA and poly(ethyl acrylate)/clay nanocomposites prepared with differ-

TABLE II
Molecular Weights and MWDs of Neat PEA and PEA Extracted from PNCs

		M_n			
Sample	Conversion (%)	Experimental	Theoretical	I_{eff}[a]	Polydispersity index
PEA	67.2	7230	6720	0.93	1.22
PNCI2	77.3	8210	7730	0.94	1.55
PNCI4	85.2	9120	8520	0.93	1.61
PNCI6	89.5	9780	8950	0.92	1.82

[a] $I_{eff} = M_n^{theo}/M_n^{exp}$, where M_n^{theo} is the theoretical number-average molecular weight and M_n^{exp} is the experimental number-average molecular weight.

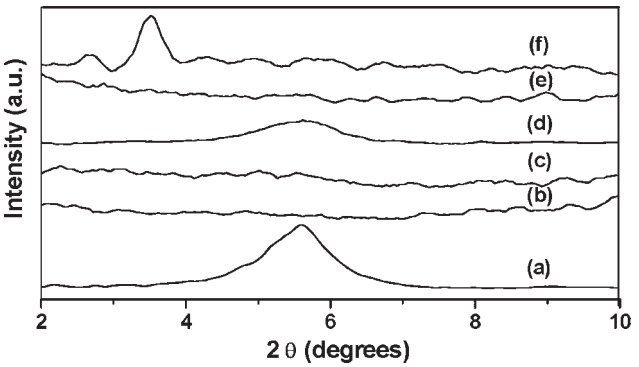

Figure 1 WAXD patterns of the PNCs: (a) nanoclay, (b) PNCI2, (c) PNCI4, (d) PNCI6, (e) PEA, and (f) PNCSL2.

ent techniques, namely, *in situ* polymerization (PNCIs) and solution blending (PNCSLs). In the *in situ* ATRP approach, there was no diffraction peak in the range of $2\theta = 2–10^\circ$ at lower clay contents [2 wt %; Fig. 1(b), 4 wt %; Fig. 1(c)] as opposed to the diffraction peak at $2\theta = 5.59^\circ$ (d_{001} spacing = 1.85 nm) for the organoclay. This suggested the probability of the complete delamination of silicate layers dispersed in the PEA matrix. However, at the same clay loading, with solution dispersion, a distinct peak appeared at $2\theta = 3.55^\circ$, which corresponded to a gallery distance of 2.89 nm [Fig. 1(f)]. This behavior was associated with an ordered intercalated morphology. In conclusion, *in situ* ATRP produced nanocomposites with a better dispersion of nanofiller compared to conventional solution blending.

At higher clay loadings in the PEA matrix prepared by *in situ* ATRP [Fig. 1(c,d)], the resultant nanocomposites exhibited a featureless XRD pattern up to 4 wt % clay content, which indicated exfoliation in the system. There was a small broad hump in the 6 wt % clay filled sample. This may have been due to the agglomeration of clays at higher filler loadings caused by their poor dispersion in the PEA matrix.

Microscopic observations

The dispersion and aggregation phenomena of organoclay within polymer matrices prepared by different approaches were compared by the EDX study of the hybrid composites, as displayed in Figure 2. The white spots over a dark background indicate the location of silicon within the hybrid composites. A uniform distribution of white spots in Figure 2(a) revealed a homogeneous dispersion of clay in PNCI2 (where the number following PNCI indicates the weight percentage of clay), whereas some local agglomeration was obtained in PNCSL2 [where the number following PNCSL indicates the weight percentage of clay; Fig. 2(b)].

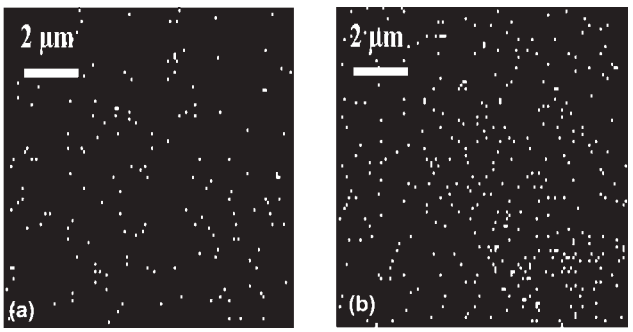

Figure 2 X-ray silicon dot mapping of the hybrid composites: (a) PNCI2 and (b) PNCSL2.

The dispersion behavior of organoclay affected the visual appearance of the hybrid composites. The composites containing Si particles predominantly as a finely dispersed phase were transparent (PNCI2), whereas the composites having some localized agglomerated Si particles were optically translucent in nature (PNCSL2).

The differences in the dispersion of clay tactoids in the nanocomposites prepared by different approaches were further examined by TEM. The white/gray areas represent the polymer–matrix phase, and the dark areas represent the organoclay. As shown in Figure 3(a), the nanocomposites prepared by solution blending had parallel stacks of clay lamella (dark contrast), and hence, this supported the intercalated structure as obtained from the XRD data [Fig. 1(f)]. Individual layers, oriented parallel to the sample sur-

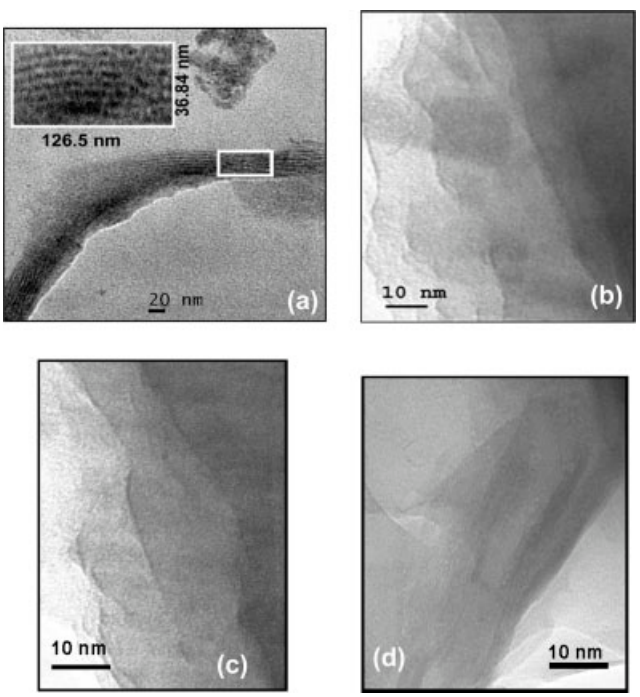

Figure 3 TEM micrographs of the PNCs: (a) PNCSL2, (b) PNCI2, (c) PNCI4, and (d) PNCI6.

face [inset of Fig. 3(a)], appeared as dark lines with an average thickness of 2.05 nm. The mean distance between the clay platelets was calculated to be 3.11 nm. For PNCI2 [Fig. 3(b)], prepared by the *in situ* ATRP approach, the TEM bright field image revealed that there were mostly well-dispersed silicate layers with an average interlayer distance larger than 10 nm. The clay layers were at different angular dispositions because of the significant disruption of organoclay tactoids. This delineated an exfoliated morphology for the PNCI2 sample. This observation was consistent with that made from the XRD pattern given in Figure 1(b). A similar type of delaminated morphology was observed in PNCI4 [Fig. 3(c)], whereas in PNCI6, clay particles showed some local agglomeration [Fig. 3(d)].

It is now interesting to discuss why PNCI produced exfoliated structures but PNCSL registered an intercalated one. The high degree of exfoliation in PNCI may be attributed to two factors: (1) first, the polar nature of matrix, which made for favorable interactions with the hydroxyl group of the clay surface and that present in the surfactant and (2) second, the low chain length of the polymer (as indicated by their molecular weights; Table II) because of which it easily penetrated between the silicate layers and thereby peeled out the clay tactoids. For the solution-blended system, we speculated that the viscosity of the final polymer hindered its efficient penetration between the gallery spacing. This led only to an interlayer expansion of clay tactoids, and consequently, an intercalated structure is produced. This result was consistent with a previous report[32] where a comparative study was made on the properties of poly(methyl methacrylate)–clay nanocomposite materials prepared by *in situ* emulsion polymerization and solution dispersion. The *in situ* system was reported to exhibit an exfoliated morphology, whereas the hierarchical structure of clay tactoids was observed to be retained in the latter case.

The TEM results were quite consistent with the WAXD study, which also registered an intercalated morphology for the solution-blended system, whereas the *in situ* ATRP system indicated an exfoliated one.

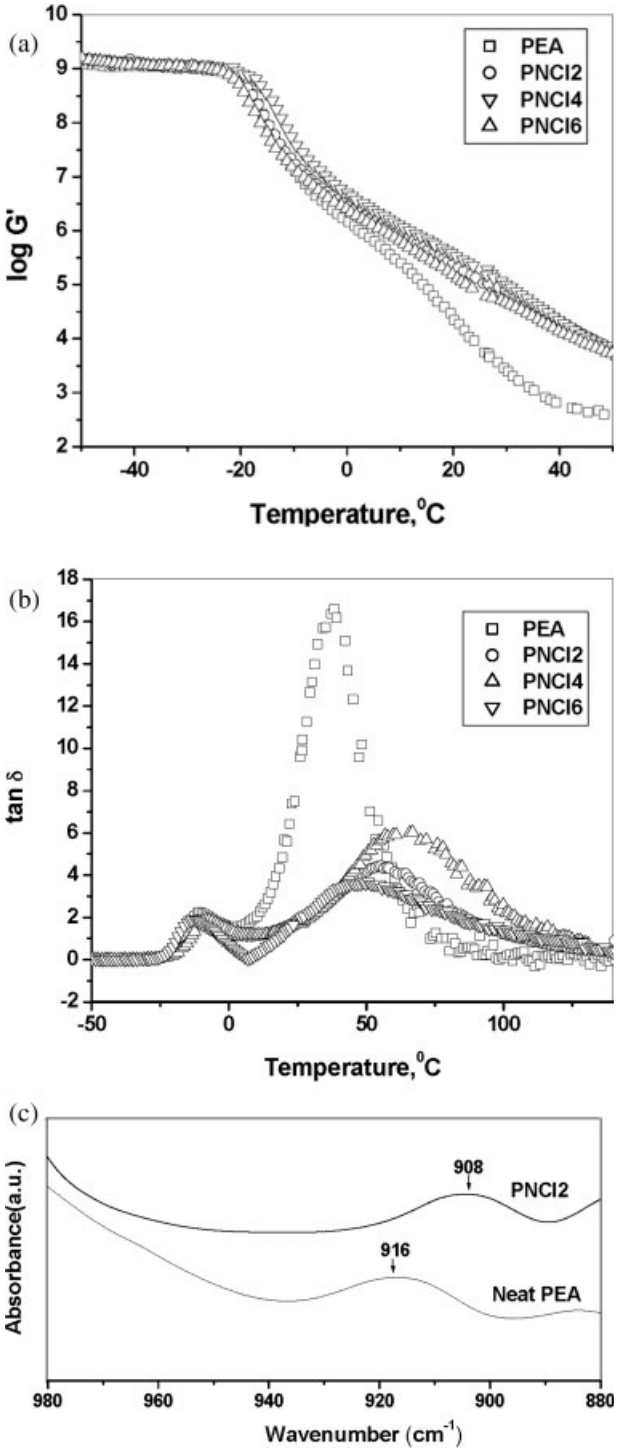

Figure 4 (a) log G' versus temperature plot of the neat polymer and nanocomposites, (b) tan δ versus temperature plot of the neat polymer and the nanocomposites, and (c) Fourier transform infrared spectra of PEA and its nanocomposite at 2 wt % clay loading.

Dynamic mechanical properties

Figure 4(a,b) reveals the temperature dependence of G' and tan δ for the virgin polymer and three PNCs with various clay loadings (2–6 wt %). G' relates the ability of the material to store energy when an oscillatory force is applied to the specimen, and tan δ, the ratio of G'' to G', relates to the molecular mobility. The mechanical reinforcement of clay in the PNCs can be visualized well from the G' data in Table III, where the G' of PEA and PNCs is presented at different temperatures. As shown in Table III, it was apparent that there were increases in G' for PNCI 4 of 8.4% at 0°C, 31.9% at 25°C, and 36.5% at 60°C. For PNCI2 and PNCI6, the reinforcement effect was smaller than that of PNCI4.

TABLE III
Summary of the Dynamic Mechanical Properties of PNCs

			Log G' (Pa)			tan δ		
Sample	T_{ll} (°C)	T_g (°C)	0°C	25°C	60°C	T_g	25°C	60°C
PEA	37.8	−10	6.18	3.87	2.48	2.23	8.22	3.86
PNCI2	55.2	−10	6.47	5.11	3.39	1.88	1.86	4.16
PNCI4	63.3	−8	6.70	5.32	3.41	1.89	1.71	5.89
PNCI6	46.1	−12	6.40	4.87	3.38	1.88	2.35	3.23

The large reinforcement effect happened because the clay tactoids were in an exfoliated state, and this made for favorable interaction with the polymer matrix, as discussed earlier. At high clay loading (PNCI6), some agglomeration of clay tactoids occurred, which led to a weaker reinforcement effect than for PNCI4.This phenomena was also clear from the XRD and TEM data (Figs. 1 and 3).

As shown in Fig. 4(a), it was clear that G' of all the PNCs increased over that of virgin PEA, although this enhancement appeared in different magnitudes at various temperatures. With an increase in temperature, however, G' decreased at each case but not in a linear manner. This may have been better represented by two breaks, one around −22°C and the other around 10°C. These two breaks were better observed in the tan δ versus temperature plot [Fig. 4(b)], which showed two different transitions in each sample. The lower temperature peak may be termed the α-transition temperature, which arose from the relaxation of the main backbone chain and corresponded to T_g of the matrix polymer. The secondary transition may be termed the liquid-liquid-transition temperature (T_{ll}), which was proposed to be attributed to the shifting of the entire molecule by cooperative segmental motion.[33] The T_g and T_{ll} values are presented in Table III. As shown clearly in this table, the T_{ll} values increased with clay content up to 4 wt %, beyond which it decreased. The T_g value was affected in the presence of clay for PNCI4, which might have been due to the presence of highly exfoliated clay particles. At still higher clay contents (PNCI6), the plasticizing effect of clay may have been operative, which subsequently decreased T_g of the matrix polymer.

In this case, because the chain length of the polymer was designed to be low (targeted DP = 100), the restriction of the segmental Brownian motion of the polymer chains was not much affected in the nanocomposites except in the highly exfoliated system (PNCI4). Again, because of the short chain length of the polymer, the effect of the pendant group was very prominent, as observed by the strong secondary transition peak at 38°C. Interestingly, there was a significant effect of clay tactoids on this secondary transition (T_{ll}); positive shifts in the peak temperature were observed for PNCI2 (17°C), PNCI4 (26°C), and PNCI6 (11°C). A dramatic decrease in the tan δ peak height at T_{ll} was noticed in these PNCs compared to the pristine polymer [Fig. 4(b)]; PNCI4 registered a 175% decrease in maximum tan δ, whereas this decrease was 359% for PNCI6. To explain this remarkable decrease in viscous response along with the peak shift to a higher temperature, we propose that the —OH group of the clay layers may have gotten anchored to the >C=O group of the pendant acrylate moiety, which led to suppression of the mobility of this pendant group to such a large extent.

This interaction was further confirmed by the shift in the IR peak [Fig. 4(c); from 916 cm^{-1} in PEA to 908 cm^{-1} in PNCI2] to lower wave-number values corresponding to the Al—O—H bending motion of the inner-surface hydroxyl group.[34]

Rheological behavior

Figure 5 shows a logarithmic plot of the steady-state shear viscosity (η_{app}) versus shear rate (γ_{app}) for neat PEA and its nanocomposites at 30°C. Inspection of the figure reveals a significant difference; the viscosities of the PNCs were much higher (ca. a twofold increase in PNCI2 and ca. a threefold increase in PNCI4 and PNCI6) than that of neat PEA. Interestingly, at similar clay contents (2 wt %), the polymer nanocomposite prepared by solution blending

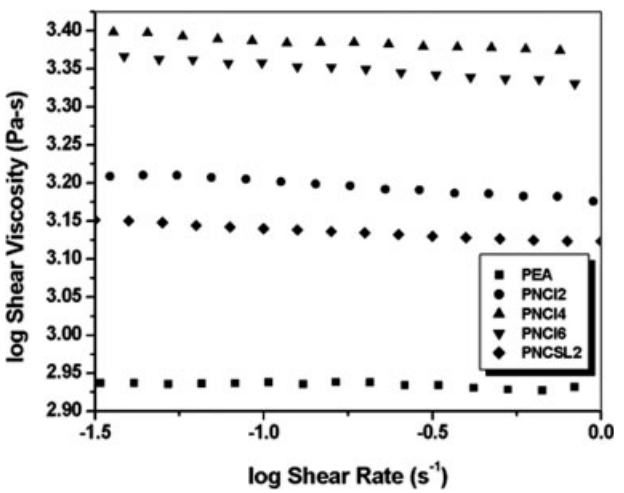

Figure 5 Plot of the log shear viscosity versus log shear rate of PEA and its nanocomposites at 30°C.

(PNCSL2) showed inferior properties to that prepared by the *in situ* method.

For comparison, we measured the rheological properties of the pristine polymer (molecular weight = 7520, polydispersity index = 1.9) and its *in situ* nanocomposite (at a 4 wt % clay loading) prepared by conventional radical polymerization with benzoyl peroxide as the initiator at 90°C.[35] With the tool of the *in situ* ATRP method, polymer/clay nanocomposites can be prepared with predetermined molecular weights and narrow polydispersity indices, whereas in the conventional polymerization system, no such control can be achieved over the resulting polymer, which generally bears a very broad MWD. The polymerization was continued only for about 2 min to keep its molecular weight low because the polymerization was not controlled, and the mass became viscous very soon. In the conventional system, the nanocomposite (at a 4 wt % clay loading) registered an improvement in shear viscosity of 8% (over the neat polymer) at a shear rate of 0.0312 Pa s, and the shear viscosity decreased with increasing shear rate. This improvement in shear viscosity decreased to 3% at a shear rate of 0.488 Pa s. On the other hand, for the *in situ* ATRP system, a constant viscosity difference (between the neat polymer and its nanocomposites) was maintained at various shear rates (Fig. 5). At a similar clay loading, the resulting nanocomposite (PNCI4) exhibited a much higher degree of enhancement in shear viscosity (by 15% over the neat polymer) compared to the conventional system. As this is the subject of a separate elaborate study that does not fit under the title of the current article, we have not carried out an extensive investigation with the conventional polymerization approach.

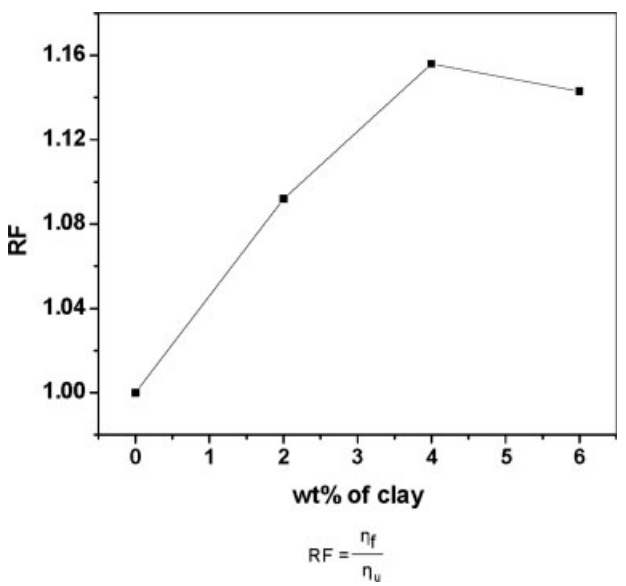

Figure 6 Plot of RF versus the weight percentage of clay hybrid nanocomposites at 30°C at a shear rate of 0.125 Pa s.

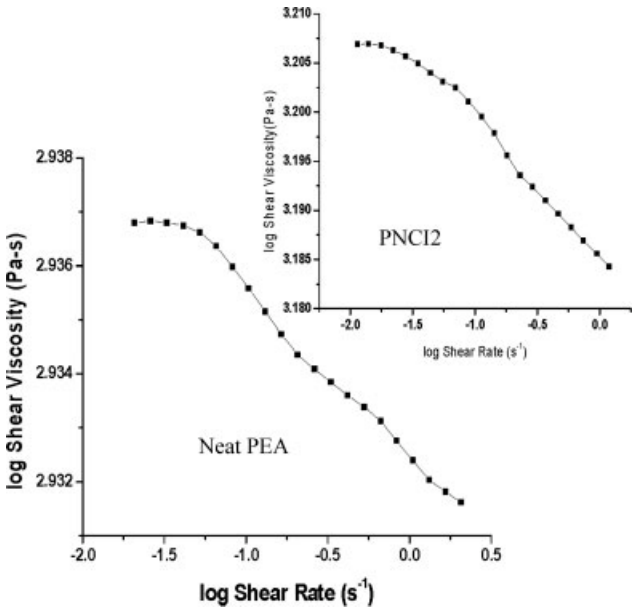

Figure 7 Plot of the log shear viscosity versus log shear rate showing the shear thinning effect of PEA and PNCI2 at 30°C.

The reinforcement factor (RF) of the PNCs was calculated by the following equation:

$$RF = \eta_f/\eta_u \quad (6)$$

where η_f is the viscosity of the nanocomposite and η_u is the viscosity of the unfilled polymer. The significance of RF is to explain the extent of reinforcement that is achieved by the dispersion of the nanoclay within the polymer matrix and is consequential to the ratio of the shear viscosity of the respective samples under identical conditions.

Figure 6 displays the RF values of the PNCs against the weight percentage of nanoclay at a particular shear rate of 0.125 Pa s. With clay loading, RF increased and became optimum at PNCI4; beyond this, it decreased (PNCI6) due to agglomeration of clay tactoids in the matrix. The large specific surface area of the organoclay nanoparticles upon exfoliation led to a significant increase in the melt viscosity of the PEA/organoclay nanocomposite.[36] Synergistically, the high shear viscosities exerted a significant stress on the clay tactoids, and consequently, it sheared the thicker stacks into smaller ones. The exfoliation of PNCs was confirmed from WAXD and TEM images, as discussed earlier. Nanosilica has a similar type of reinforcing effect on the polymer matrix, as reported in an earlier article from our laboratory.[37]

A marginal decrease in shear viscosity was obtained with increasing shear rate for all the systems, as indicated in Figure 7, where the data from Figure 5 (on the *y* axis) are plotted on a magnified scale. The plots registered a shear thinning effect for PNCI2, including the virgin polymer, which obeyed

TABLE IV
***n* and *k* Values of Different Samples**

Sample	n	$k \times 10^{-2}$ (Pa s)
PEA	0.99	8.55
PNCI2	0.98	15.20
PNCI4	0.98	23.55
PNCI6	0.98	21.57

the power law equation. The other PNCs followed a similar trend. The k and n values of the systems [when eqs. (1)–(5) were applied], as calculated from the viscosity versus shear rate traces, are included in Table IV. The values showed that the virgin PEA exhibited almost Newtonian fluid behavior ($n \sim 1$), and the filled samples exhibited marginally non-Newtonian behavior and became slightly pseudoplastic in nature. The activation energy of flow for the PNCs is plotted against the shear rate in Figure 8. The activation energy of all of the PNCs was higher than that of PEA and increased monotonically with clay loading, which indicated a higher resistance to flow. This accounted for the higher viscosity in the PNCs compared to the virgin polymer PEA. The activation energy values were almost constant for PEA over the range of shear rates, whereas a decreasing trend was observed in the PNCs.

TGA

Figure 9(a) displays typical TGA thermograms of weight loss as a function of temperature for neat PEA and the PNCs as measured under a nitrogen atmosphere. It was apparent that all of the PNCs had a greater thermal stability than neat PEA, and PNCI4 exhibited the highest stability. The onset of degradation, as measured from the intersection of the tangent of the initial part and the inflection part, are registered in Table V. The corresponding differential thermogravimetric curves (DTG) in Figure 9(b) clearly showed that the thermal degradation reaction was highly retarded in the presence of clay (rate of degradation = 3.24%/°C for the pristine polymer, 3.13%/°C for PNCI2, 2.94%/°C for PNCI4, and 2.17%/°C for PNCI6). Also, with increasing clay content, a marginal shift in the degradation peak (peak maximum

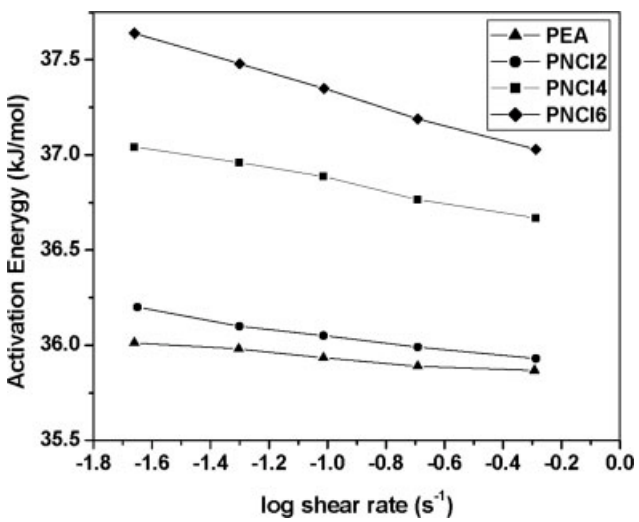

Figure 8 Activation energy versus shear rate for PEA and its nanocomposites.

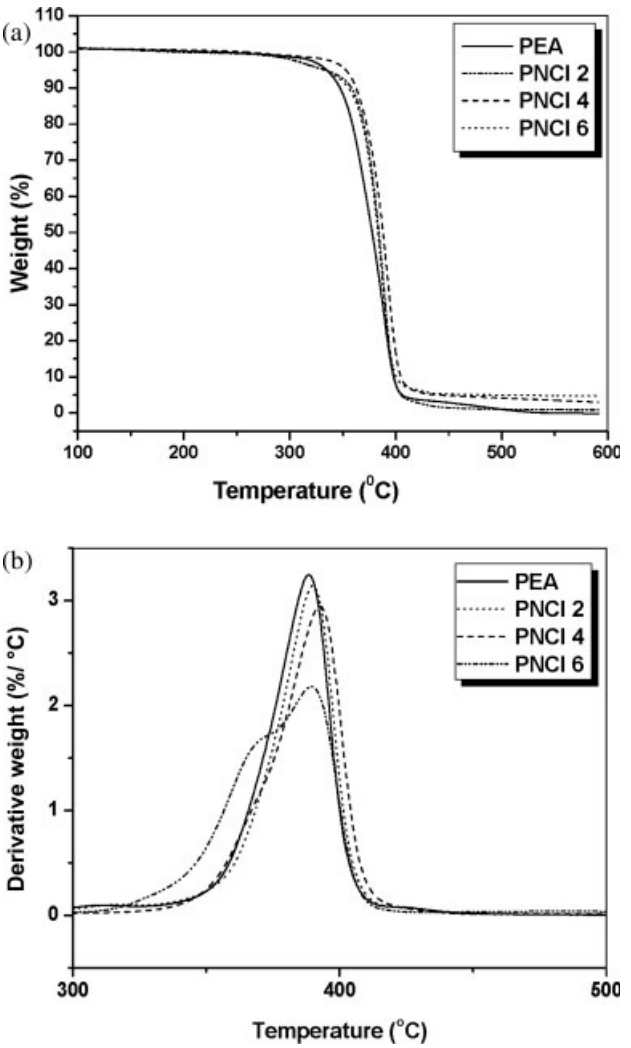

Figure 9 (a) TGA thermograms and (b) DTG thermograms of PEA and its nanocomposites at different clay loadings.

TABLE V
Results of TGA

Sample	Degradation peak		Residue (wt %)
	Peak maximum temperature (°C)	Onset temperature (°C)	
PEA	388	355	0.36
PNCI2	389	369	0.81
PNCI4	392	371	3.07
PNCI6	389	367	4.70

temperature) was observed toward higher temperatures. At a very high clay content (6 wt %), a two-stage degradation was observed. This was due to the higher clay content in this case, and a competitive degradation may have occurred between the organic modifier and the polymer matrix. Cloisite 30B, the clay used here, was degraded under similar conditions and exhibited a two-stage degradation behavior. The corresponding DTG curve showed the initial peak at the same temperature where the first peak of PNCI6 arose. The residual weight was higher in the PNCs than in PEA, which certainly indicated that the PNCs were more stable than the neat polymer. To account for this enhanced thermal stability, we suggest that in the PNCs, the clay particles acted as heat sinks and prevented the degradation of the polymers.

CONCLUSIONS

Tailor-made PNCs with predictable molecular weights and narrow polydispersity indices were prepared at different clay loadings by *in situ* ATRP and solution blending. The *in situ* approach was proven to be the better option, as it provided an exfoliated morphology, as shown by WAXD and TEM. On the contrary, conventional solution blending led to only interlayer expansion of the clay gallery.

The mechanical reinforcement of the clay in the PNCs could be visualized from the dynamic mechanical thermal analysis and rheometric data. For example, at 60°C, PNCI4 exhibited a 36.5% improvement in G' compared to the pristine polymer sample. A 4 wt % loading was found to be the optimum one, beyond which the agglomeration of clay tactoids occurred, which led to the deterioration of the properties. From the tan δ plot, it was interesting to observe that the mobility of the pendant acrylate moiety (as indicated for T_{ll} at 38°C) was highly affected in the presence of nanoclay, whereas Brownian motion of the main backbone chain remained almost unaffected. This interaction was further confirmed by Fourier transform infrared analysis.

The melt viscosities of the nanocomposite samples were significantly higher than those of the control samples. The k and n values showed that the virgin PEA exhibited almost Newtonian fluid behavior, and the filled samples registered marginally non-Newtonian behavior and, thereby, became pseudoplastic in nature. The activation energy of all of the PNCs is higher than that of PEA and increased monotonically with clay loading, which indicated a higher resistance to flow.

The thermal stability of the nanocomposites increased distinctly, as indicated by the shift in peak maximum temperature (388 and 392°C for the neat polymer and PNCI4, respectively)and the decrease in the rate of degradation (3.24%/°C for the pristine polymer, 3.13%/°C for PNCI2, 2.94%/°C for PNCI4, and 2.17%/°C for PNCI6).

References

1. Pinnavaia, T. J.; Beall, G. W. Polymer–Clay Nanocomposites; Wiley: New York, 2000.
2. Alexandre, M.; Dubois, P. Mater Sci Eng 2000, R28, 1.
3. Messersmith, P. B.; Giannelis, E. P. J Polym Sci Part A: Polym Chem 1995, 33, 1047.
4. Zeng, C.; Lee L. J. Macromolecules 2001, 34, 4098.
5. Maiti, M.; Bhowmick, A. K. J Polym Sci Part B: Polym Phys 2006, 44, 162.
6. Patel, S.; Bandyopadhyay, A.; Ganguly, A.; Bhowmick, A. K. J Adhes Sci Tech 2006, 20, 371.
7. Vaia, R. A.; Giannelis, E. P. Macromolecules 1999, 30, 7990.
8. Vaia, R. A.; Giannelis, E. P. Macromolecules 1997, 30, 8000.
9. Balazs, A. C.; Singh, C.; Zhulina, E. Macromolecules 1998, 31, 8370.
10. Ginzburg, V. V.; Balazs, A. C. Macromolecules 1999, 32, 5681.
11. Ginzburg, V. V.; Singh, C.; Balazs, A. C. Macromolecules 2000, 33, 1089.
12. Vaia, R. A.; Vasudevan, S.; Krawiec, W.; Seaulon, L. G.; Giannelis, E. P. Adv Mater (Weinheim, Germany) 1995, 7, 154.
13. Furuichi, N.; Kurokawa, Y.; Fujita, K.; Oya, A. J Mater Sci 1996, 31, 4307.
14. Weimer, M. W.; Chen, H.; Giannelis, E. P.; Sogah, D. Y. J Am Chem Soc 1999, 121, 1615.
15. Bottcher, H.; Hallensleben, M. L.; Nuß, W. H.; Bauer, J.; Behrens, P. J Mater Chem 2002, 12, 1351.
16. Zhou, Q.; Fan, X.; Xia, C.; Mays, J.; Advincula, R. Chem Mater 2001, 13, 2465.
17. Zhao, H.; Shipp, D. A. Chem Mater 2003, 15, 2693.
18. Zhao, H.; Argoti, S. D.; Farell, B. P.; Shipp, D. A. J Polym Sci Part A: Polym Chem 2004, 42, 916.
19. Clercq, B. D.; Laperre, J.; Ruys, L. Prog Org Coat 2005, 53, 195.
20. Yasuhiro, F.; Takehiro, I. Jpn. Pat. JP 91-24161 19910124.
21. Eiju, K.; Goro, I.; Akio, S. Jpn. Pat. JP 88-97817 19880420.
22. Fung, W. Coated and Laminated Textiles; CRC: Cambridge, England, 2002.
23. Wang, J. S.; Matyjaszewski, K. J Am Chem Soc 1995, 117, 5614.
24. Kato, M.; Kamigaito, M.; Sawamoto, M.; Higashimura, T. Macromolecules 1995, 28, 1721.
25. Matyjaszewski, K. In Controlled Radical Polymerization; Matyjaszewski, K., Ed.; ACS Symposium Series 685; American Chemical Society: Washington, DC, 1998.
26. Matyjaszewski, K.; Xia, J. Chem Rev 2001, 101, 2921.
27. Percec, V.; Barboiu, B. Macromolecules 1995, 28, 7970.
28. Lee, S. S.; Ma, Y. T.; Rhee, H. W. Kim J. Polymer 2005, 46, 2201.
29. Datta, H.; Bhowmick, A. K.; Singha, N. K. J Polym Sci Part A: Polym Chem 2007, 45, 1661.
30. Fox, T. G.; Gratch, S.; Loshack, S. In Rheology—Theory and Applications; Eirich, F. R., Ed.; Academic: New York, 1956; Vol. 1.
31. Yu, Y. H.; Lin, C. Y.; Yeh, J. M.; Lin, W. H. Polymer 2003, 44, 3553.
32. Yeh, J. M.; Liou, S. J.; Lai, M. C.; Chang, Y. W.; Huang, C. Y.; Chen, C. P.; Jaw, J. H.; Tsai, T. Y.; Yu, Y. H. J Appl Polym Sci 2004, 94, 1936.
33. Ferry, J. D. Viscoelastic Properties of Polymers; Wiley: New York, 1961.
34. Wada, K. Clay Miner 1967, 7, 51.
35. Datta, H.; Singha, N. K.; Bhowmick, A. K. Rubber Technology Centre, Indian Institute of Technology, Kharagpur, 2007.
36. Jeon, H. S.; Rameshwaram, J. K.; Kim, G.; Weinkauf, D. H. Polymer 2003, 44, 5749.
37. Bandopadhyay, A.; Sarkar, De, M.; Bhowmick, A. K. Rubber Chem Technol 2005, 78, 806.